Audiological Medicine, 2010; 8: 120–128

informa
healthcare

ORIGINAL ARTICLE

Three-dimensional confocal microscopy of the mammalian inner ear

GLEN H. MACDONALD & EDWIN W RUBEL

Virginia Merrill Bloedel Hearing Research Center, Department of Otolaryngology-HNS, University of Washington, Seattle, WA, USA

Abstract

Objective: Control the refractive index in fixed specimens of mammalian inner ear to reduce spherical aberrations that limit our ability to obtain 3-dimensional images of fluorescently labeled inner ear specimens by conventional laser scanning confocal microscopy. *Study Design:* Mouse inner ear specimens were fixed with minimal dissection, rapidly decalcified and fluorescently labeled by immunohistochemistry then impregnated by epoxy resin or a clearing agent composed of 5 parts methyl salicylate:3 parts benzyl benzoate. The specimens were imaged by both confocal microscopy and by widefield epi-fluorescent microscopy, with additional processing by deconvolution. *Results:* Rapid decalcification preserved tissue morphology and antigenicity for the antibodies tested. Although the epoxy allowed some reduction of spherical aberration, the clearing agent enabled optical volumes of high quality and resolution to be collected through the inner ear. The conditions for immunolabeling are important to ensure adequate perfusion of the immuno-labeling reagents throughout the specimen. *Conclusion:* Spherical aberration reduces signal intensity, contrast and resolution in optical microscopy. Creating a homogeneous refractive index throughout the inner ear to reduce spherical aberration allowed optical volumes to be collected through an intact, fluorescently labeled cochlea in a manner limited by the working distance of the objective lens rather than by spherical aberration. Optical volumes collected by this method from the mammalian inner ear promise to be useful for applications such as tracing innervation patterns, counting sensory cells or other structures over large regions of the sensory epithelium, and characterization of the inner ear in animal models of human deafness disorders.

Key words: *fluorescence, inner ear, refractive index, spherical aberration*

Introduction

This manuscript expands upon an abstract presented at the XIV International Symposium in Audiological Medicine that described our published work utilizing an epoxy resin or a clearing agent composed of methyl salicylate and benzyl benzoate to reduce spherical aberration in inner ear specimens for confocal microscopy. New methodological details in our labeling protocols are presented, along with an attempt to summarize the importance of the optical properties of the specimen for light microscopy.

Light microscopy can produce aberration-free images only when the specimen possesses specific optical properties. A typical research-grade dry or oil-immersion objective lens for high-resolution imaging assumes that the specimen preparation possesses a uniform refractive index (RI) of 1.518 (approximating immersion oil) and is mounted with a coverslip thickness of 0.17 mm with an RI of approximately 1.523 (1). Deviations from these conditions result in lateral displacement of the outer converging light rays, relative to those that pass nearer to the optical axis, to create spherical aberration by enlarging the point-spread function. Spherical aberration results in signal loss, reduced resolution and lower image contrast. The major cause of spherical aberration in fluorescent microscopy is RI non-uniformity, or a mismatch between the RI of the specimen and the specimen RI for which the objective was designed (2,3).

Traditionally, preparative methods for temporal bone structures constrain the occurrence of spherical aberration by sectioning or microdissection to minimize the amount of tissue in the optical path. Although these approaches have produced high-quality two-dimensional images, they are labor intensive,

Correspondence: E. W Rubel, Virginia Merrill Bloedel Hearing Research Center, Department of Otolaryngology-HNS, Box 357923, University of Washington, Seattle, Washington 98195, USA. (Tel) +1-206-616-8360 (Fax) +1-206-221-5685 E-mail: rubel@uw.edu

(Accepted 11 June 2010)

ISSN 1651-386X print/ISSN 1651-3835 online © 2010 Informa Healthcare
DOI: 10.3109/1651386X.2010.502301

may distort the tissue and much additional processing is required to create a three-dimensional representation of the inner ear by reconstruction from a series of two-dimensional images.

Previous work in our laboratory obtained three-dimensional images by confocal microscopy from bisected adult mouse cochlea embedded in epoxy resin (4). Although this was an improvement over reconstruction from sections, an acceptable fluorescent signal could be obtained only through a portion of the working distance of any objective lens employed.

We have now obtained three-dimensional images of the mature mammalian inner ear with confocal microscopy by creating a homogeneous refractive index throughout this complex structure (5). The clearing agent is composed of 5 parts methyl salicylate: 3 parts benzyl benzoate (MSBB), and was initially described as part of an array of clearing agents used to aid in the microscopy of specific animal tissues (6). It was initially applied to the mammalian cochlea for orthogonal plane fluorescent optical sectioning (OPFOS) (7,8), a sheet-illumination imaging method. It was subsequently used with high-resolution OPFOS (9,10) and more recently employed for thin-sheet laser illumination microscopy (TSLIM) (11).

We show that it is possible to obtain confocal volumes up to 900 μm in thickness through an intact, fluorescently labeled cochlea utilizing a low NA objective. Minimal dissection allows high NA objective lenses to record optical volumes limited by the working distance of the objective lens, rather than by spherical aberration created by the specimen.

Materials and methods

Inner ears were collected from mice raised in the University of Washington vivarium in accordance with IACUC regulations. The mice, 129/CBA, were killed by cervical dislocation at ages ranging from post-natal day 7 (P7) to adult. Each temporal bone was dissected to expose the cochlea, the stapes was removed and a small hole made in the apex of the cochlea, over the helicotrema. A slow perfusion of 0.1 ml 4% paraformaldehyde buffered with 0.1 *M* sodium-potassium phosphate, pH 7.4, was followed by an overnight post-fixation in 4% paraformaldehyde at 4°C, on a nutator.

The specimens were washed with 0.01 *M* sodium-potassium phosphate buffer, pH 7.4, containing 0.9% sodium chloride (PBS), three times for 10 min each, with gentle rotation at room temperature. Each specimen was placed in a polystyrene Petri dish, covered with PBS, and gently dissected free of extraneous soft tissues while viewed under a dissecting microscope (MZ-8, Leica Microsystems, Wetzlar, DE) with oblique illumination from a 150-W fiberoptic illuminator (Techniquip, Livermore, CA). Enough bone was removed from the cochlea to allow it to lie on its lateral or ventral side. Circulation of the immunolabeling reagents through the inner ear was encouraged by opening the round window, dissecting a hole in the bone overlying the lower turn and enlarging the hole in the apical turn.

In our published protocol (5), decalcification was accomplished by submerging specimens for three days in 10% ethylenediamine tetra-acetic acid-disodium salt (EDTA, Sigma, St. Louis, MO) in PBS, pH 7.4, at 4°C, with rocking. The EDTA was removed by rinsing with three changes of PBS, 10 min each, at room temperature with rotation.

Recently, specimens were prepared with a rapid decalcification by means of 15-min immersion in RDO Rapid Decalcifier (Apex Engineering Products Corp., Aurora, IL) at room temperature, with gentle rotation. The RDO was removed with three rapid exchanges of PBS followed by three changes of PBS for 5 min each, at room temperature, with rotation.

Immunocytochemistry

This labeling protocol employed a rocking platform ('nutator') to circulate reagents. However, the quality and consistency of labeling are controlled by the interplay of agitation force, vessel dimensions, reagent volume and degree of dissection. The incubation vessel required sufficient inner diameter to allow a noticeable wave action on the reagent surface. A reagent volume of 1 ml in a 4-ml glass vial with a polyethylene snap cap (Cat. No. 225532, Wheaton, Millville, NJ) incubated on a nutator (Model 260100F, Fisher Scientific, Pittsburgh, PA) provided acceptable labeling without allowing the specimens to tumble in a damaging manner. The plastic snap-on caps were resistant to the clearing agent. A volume of 1 ml was sufficient to keep the specimens submerged to avoid entrapment of air bubbles that may block the flow of reagents within the cochlear duct. Note that the MSBB mixture will dissolve polystyrene dishes (as well as computer keyboards and microscope focus knobs).

Decalcified specimens were transferred into the 4-ml glass vials with up to four inner ears per vial. All labeling incubations were carried out at 4°C, with agitation on the nutator, and rinses were carried out at room temperature, on a platform rotator, unless otherwise noted. The inner ears were incubated in a minimal volume of Image-iT FX (Molecular Probes, Eugene, OR) for 30 min at room temperature, on a rotator, to reduce interactions between fluorophores and tissue. This was replaced with an immuno-block solution of PBS containing 10% normal serum (Vector Laboratories, Burlingame,

CA), 0.5% bovine serum albumin (A-7030, Sigma, St. Louis, MO) and 0.1% Triton X-100 (Sigma). The immuno-block was removed after an incubation of 4 h carried out at room temperature, with rotation. The specimens were covered with 1 ml of immuno-block containing the primary antibodies and incubated for three days. The primary antibodies employed in this report were mouse monoclonal anti-parvalbumin (MAB1572, Chemicon, Temecula, CA) and chicken anti-200 kD neurofilament (AB5539, Chemicon) diluted 1/500 in immuno-block solution as a 'cocktail' mixture.

After incubation, the primary antibodies were removed and the specimens were washed three times in PBS for 2 h each. The final PBS wash was replaced with a 1-ml volume of immuno-block solution containing the secondary antibodies, each diluted 1/500, and the nucleic acid label DAPI (Sigma) at a concentration of 0.2 μg/ml, and then the specimens were incubated for three days. Secondary antibodies employed were goat anti-mouse IgG conjugated to Alexafluor 488 and goat anti-chicken IgY conjugated to Alexafluor568 (Molecular Probes). The inner ears were washed three times with PBS, 2 h each, at the end of incubation.

Clearing and mounting

The labeled inner ears were dehydrated with a graded series of ethanol from 70% through absolute ethanol, as previously described. They were transferred into a clearing medium made of 5 parts methyl salicylate and 3 parts benzyl benzoate (MSBB). The RI of this clearing mixture was calculated to be 1.556 by multiplying the proportion of each reagent in the final mixture by its RI and summing the results.

Each cleared specimen was mounted for imaging by placement in an imaging chamber and covering by several drops of MSBB. An imaging chamber was created by attaching a 24-mm × 50-mm coverslip to a 25-mm × 75-mm × 1-mm aluminum frame slide containing a large central opening. These slide frames had been used to support plastic films used for laser microdissection. The film was scraped off with a razor blade and residual glue removed with absolute ethanol. The coverslips were measured to be of 170–173 μm thickness by means of a micrometer with an accuracy of 1 μm (No. 293-765-30, Mitutoyo America, Aurora, IL) and attached with silicone aquarium sealant (All-Glass Aquarium Co., Franklin, WI). If desired, a second frame could be attached to the side opposite the coverslip in order to create a chamber 2 mm deep to allow greater volume of clearing agent or to provide clearance for a cover over the chamber to reduce evaporation. The silicone sealant was allowed to dry for 24 h under a weight, then the frame was inverted so that the coverslip became the floor of a specimen chamber (Figure 1).

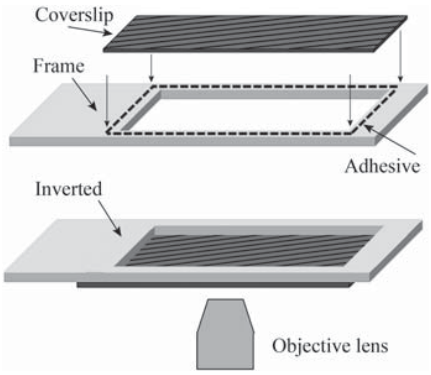

Figure 1. A specimen holder was fabricated from an aluminum frame originally used to support laser microdissection specimen films. The completed holder is flipped over after attaching the coverslip to create a sealed depression in which the specimen is placed.

Each specimen was placed in the imaging chamber, covered with a few drops of clearing agent, and positioned while observing under a dissecting microscope. Fragments of coverglass were sometimes employed as shims to maintain the position of the cochlea. Microscopy of the organ of Corti using high-NA objectives with short working distances required that the side of the cochlea be sliced off in a plane roughly parallel to the modiolus to remove the lateral portion of the cochlear duct. This was accomplished by placing the specimen in a Petri dish containing a layer of clear silicone rubber (Sylgard 184, K.R. Anderson Co., Morgan Hill, CA) and slicing the cochlear shell with a scalpel blade.

Confocal microscopy

Mounted specimens were viewed on a Fluoview-1000 laser scanning confocal microscope with an IX-81 inverted microscope (Olympus America, Center Valley, PA). The fluorescent labels DAPI, AlexaFluor 488, AlexaFluor 568 and AlexaFluor 660 (not shown) were observed using laser lines of 405 nm, 488 nm, 561 nm and 635 nm, respectively, for excitation. Dichroic mirrors and bandpass emission filters used for the four fluorescence detectors on this instrument were 490 nm longpass dichroic and 425–475 nm bandpass interference filter, 560 nm longpass dichroic and 500–560 nm bandpass interference filter, 640 nm longpass filter and 575–640 bandpass interference filter, a front surface mirror and 655–755 nm bandpass interference filter, respectively. The specimens were viewed with the following dry objectives: a 4x/NA 0.16 of 13 mm working distance, a 10x/NA 0.4 with 3.1 mm working distance and a 20x/NA 0.75 UPLSAPO with 600 μm working

distance. A 40x/NA 1.3 UPFL oil-immersion objective lens with 200 µm working distance was also employed. Confocal images were collected with 12-bit digitization and then saved in a 16-bit OIF format. The oil-immersion objective was used with an immersion oil of RI 1.554 (Type A, Cargille Laboratories, Cedar Grove, NJ).

Confocal image volumes were deconvolved by Huygens software (Scientific Volume Imaging, Hilversum, NL) using a constrained maximum likelihood estimate algorithm. Current work utilized Huygen Professional 3.5.5 on a Macintosh Pro computer, OS 10.6.2. Maximum intensity projections (MIP) for two-dimensional (2D) images and three-dimensional (3D) rotations were created using Huygens and ImageJ, version 1.42 (Rasband, National Institutes of Health, Bethesda, MD, http://rsb.info.nih.gov/ij/). ImageJ was used on Macintosh Intel-based computers, OS 10.6.2 (Apple, Inc., Cupertino, CA). Final figures were created with Photoshop (Adobe, San Jose, CA). All figures were subjected to histogram stretch and gamma adjustment to increase contrast.

Results

Rapid decalcification was compatible with immunocytochemical labeling

The rapid decalcification with RDO reduced the preparation time by four days without apparent degradation of immunocytochemical labeling. The resulting histology appeared indistinguishable from that achieved by long exposure to EDTA.

Altering the specimen RI reduced spherical aberration

The mouse inner ear became nearly transparent after clearing by MSBB, visible only by a brown tint in the thicker bone regions and the pigmented epithelium in the stria vascularis. Small fragments of inner ear lacking the stria vascularis, such as surface preparations containing half turns of organ of Corti, become completely transparent (data not shown). Very low power levels could be employed for confocal microscopy with these specimens. For example, the 488-nm laser line was used in the range of 2–4%, corresponding to 2.1–4.2 µW, measured at the back aperture of the objective lens. Low laser power improved image contrast through reduced light scattering and autofluorescence, as well as minimized photobleaching. The time required to collect a confocal volume was dependent upon several factors, including the lateral and axial sampling density, pixel dwell time, the use of sequential channel capture and whether averaging was employed. The images presented here were collected with a 2-µs dwell time and 800 × 800 or 1024 × 1024 pixel sampling, sequential channel collection and no averaging. A full resolution image incrementing focus at 3 µm for the 10x/NA 0.l6 objective or 0.3 µm for the 40x/NA 1.30 objective required 45–60 min to collect three channels of fluorescence. Smaller field sizes and reduced depths of focus on specific

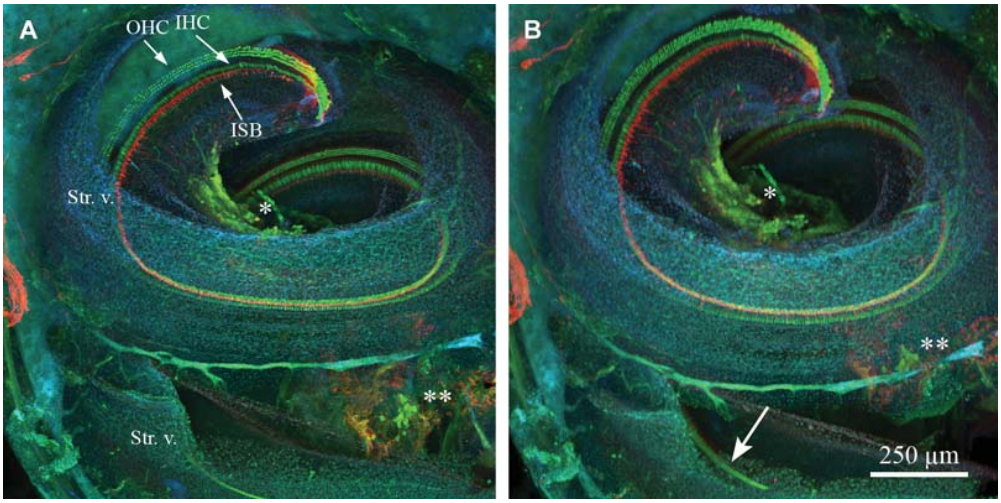

Figure 2. An inner ear oriented on its lateral side (toward the objective lens), displays the organ of Corti (}) spiraling around the modiolus through a haze of nuclei in the stria vascularis and lateral wall tissue. The IHC and OHC are labeled for parvalbumin (green) and the afferent nerve fibers are labeled for 200 kD neurofilament (red). Nuclei (blue) are labeled with the DNA label, DAPI. Neurons in the spiral ganglion near the apex (*) and at its base (**) were also labeled for parvalbumin. (A) Inner ear as imaged lying against the coverslip. (B) Same optical volume after rotating the apex 15° in the x-axis to better view the modiolus and the basal turn crossing over the round window (arrow). Maximum intensity projection from 217 image planes from a 651-µm thick optical volume, 129/CBA mouse, P33 days, 10x/0.40 objective.

structures, or reduced axial resolution (fewer focal planes) required 15–25 min.

Optical volumes viewed by digital sectioning and re-orientation

Optical volumes of the inner ear could be viewed as a maximum intensity projection in the plane at which the data were captured, or rotated to an orientation more favorable for viewing. Figure 2A provides an example in which spiral ganglion cell bodies labeled for parvalbumin, a calcium binding protein, in the apical modiolus (asterisk) were obscured by the stria vascularis in the original imaging plane, while the neurons (double asterisk) are visible at the base. Figure 2B presents the optical volume after rotation 15° around the x-axis, bringing the apex 'towards' the viewer. The apical neurons are now visible, while the basal ganglion neurons have become obscured by the stria vascularis. The rotation also makes the organ of Corti in the basal turn more visible as it passes over the round window. Optical volumes can be digitally re-sectioned along arbitrary axes to additional perspectives of the tissue. Sub-regions from within an optical volume may be extracted, as in Figure 3C, to view specific features. An image with sufficient axial resolution may be presented as a projection along any axis, such as the Y,Z axis (relative to acquisition) presented in Figure 3D.

Reduction of background in large specimens

Pre-treatment of the tissue with the Image-iT FX reagent noticeably reduced the non-specific binding of fluorescent labels to the surfaces of the cochlear duct. When present, this background label became evident when viewing through large regions of tissue and sometimes obscured details when images were adjusted to increase the contrast of small structures. Despite blocking treatments, the tectorial membrane commonly displayed a reddish hue from non-specific binding of the Alexafluor 568 label (visible in Figure 3) and small punctate deposits from all secondary antibodies. Haze from out-of-focus light and light scattering that accumulated in

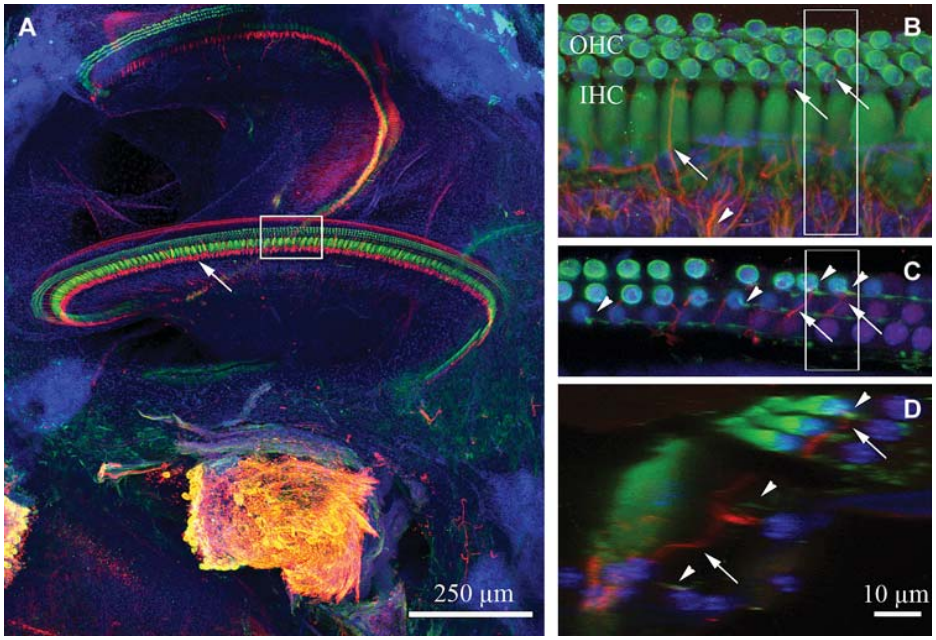

Figure 3. An inner ear imaged through the bony capsule using a 10x objective (A). Parvalbumin (green) is observed in the three rows of OHC and the single row of IHC. Nerve fibers emerging from the habenula perforata (arrow) were labeled with 200 kD neurofilament (red). The severed end of the modiolus labeling for parvalbumin and 200 kD neurofilaments creates the large yellow rosette at the bottom of this panel. The white box indicates the region subsequently imaged at high magnification (B–D). A maximum intensity projection through the organ of Corti illustrates type I afferent and efferent nerve fibers labeled for 200 kD neurofilament mixed with fibers labeled for parvalbumin (arrowhead) emerging from the habenula perforata. Some fibers pass through the IHC row towards the OHC (arrow) (B). A maximum intensity projection of a 6-µm thick layer from the OHC basal region displays synapses on the OHC by spiral fibers (arrowheads) and efferent fibers (arrows) (C). The optical volume was then digitally resectioned in the Y,Z plane through the region indicated by the white boxes in (B) and (C), then rendered into a brightest-point projection (D) to present a transverse view of the optical volume. The tunnel of Corti is crossed by an efferent fiber (arrow) and putative afferent nerve fibers (arrowheads). Synaptic structures observed in (C) are present beneath the OHC. Arrowheads indicate efferent fibers and arrows indicate probable type II afferent fibers. 129/CBA mouse, P33 days, littermate to that shown in Figure 2, 10x/0.40 objective (A), 40x/1.30 objective (B–D).

these large optical volumes was removed by deconvolution of the confocal images.

The organ of Corti can be observed through the intact cochlear shell

As the 10x/NA 0.4 objective lens possessed a 3.1-mm working distance sufficient to image the whole, it was most commonly employed for this purpose in preference to the 4x with its lower NA. The demagnification of the FV-1000 optics allowed a choice between collecting an entire cochlea within a single field of the 10x objective and using the zoom function to collect specific regions at the full resolution of the lens. Maximum intensity projections of whole inner ears tended to present a haze of fluorescently-labeled nuclei in the outer shell of the cochlea and its attached connective tissue. This is observed in Figure 2, at the periphery of the outer bone, and the blue haze in the four corners of Figure 3. Optical planes containing bone that obscured interior structures could be excluded from maximum intensity projections, as illustrated in Figure 3.

Inner ears could be imaged first through the intact cochlear shell using a 10x objective (Figure 3A), then imaged with a 40x/1.3 NA oil-immersion objective (Figures 3B–D) after the side of the cochlear shell was removed by slicing with a scalpel blade. At 10x, some large nerve bundles labeled for 200 kD neurofilament (red) were visible within the osseous spiral limbus. Most nerve fibers were strongly labeled by the antibody against 200 kD neurofilament as they emerged from the habenula perforata (Figure 3A). At this low power the inner spiral bundle (arrow) appeared as a dense tangle at the base of the IHC with only a few fibers visible as they extend through the IHC to cross the tunnel of Corti and innervate the OHC. Some fibers labeled for 200 kD neurofilament projected longitudinally for a short distance before crossing the tunnel in the manner of efferent nerve fibers. In contrast, nerve fibers exiting the habenula perforata demonstrated weak labeling intensity for parvalbumin (green) that was usually overwhelmed by the stronger labeling for 200 kD neurofilament when viewed in merged color images. A small population of nerve fibers was labeled predominately for parvalbumin, but appeared unlabeled for neurofilament (Figure 3B). Small nerve fibers resembling type II afferent fibers could also be observed crossing the tunnel of Corti and projecting longitudinally in the manner of the outer spiral bundle. Restricting the maximum intensity projection in Figure 3B to 6 μm thickness in the basal region of the OHC allowed visualization of the thin fibers of the outer spiral bundle (green), as well as their synapses on OHC (arrowheads) (Figure 3C). A few fibers strongly labeled for 200 kD neurofilament and could be observed projecting radially across the tunnel to branch and form synapses on the OHC (arrows).

A maximum intensity projection in the Y,Z plane through the volume outlined in Figures 3B and 3C displays the organ of Corti as though focusing the objective lens from the left side of the box. Afferent fibers are visible as they climb the IHC to form synapses and a possible efferent fiber is shown crossing the tunnel of Corti (arrow). A synapse visible at the outermost row of OHC (arrow) is also identified in Figure 3B and Figure 3C. A small nerve fiber labeled predominately for parvalbumin (arrowhead) crosses near the floor of the tunnel of Corti and small cross-sections of outer spiral bundle fibers labeled for parvalbumin are visible below the OHC and Deiters cells. A synapse from such a fiber is present on the base of the outermost OHC (arrowhead). These images at high magnification demonstrate the superior preservation of morphology possible with this method and the ability to create 3D images at high resolution.

Discussion

Our prior work (4) obtained optical volumes to a thickness of 300 μm from mammalian cochlear tissue using a 4x 0.1 NA objective and to 60 μm thickness using an oil-immersion objective of 60x/1.4 NA. The progressive decrease of signal intensity, contrast and resolution limited the thickness of our confocal volumes to much less than the working distance of the objective lenses. Since the estimated RI of epoxy resin was 1.49, we sought to increase the refractive index in our specimens to further reduce spherical aberration.

The MSBB clearing agent was first employed to reduce spherical aberration in the mammalian cochlea for imaging by OPFOS (7). MSBB rendered the specimen sufficiently transparent to record images of inner ear interior structures through the intact bony capsule of the guinea pig inner ear and was subsequently used to clear the mouse inner ear for other sheet illumination methods (9–11). We applied MSBB to conventional laser scanning confocal microscopy on the mouse inner ear (5) and found that spherical aberration and light scattering within the specimen was reduced sufficiently to allow the working distance of the objective lens to become the limiting factor in focus depth.

Spherical aberration increases with the third power of the NA of the objective lens, the degree of RI mismatch and the depth of focus into the specimen. Major sources of spherical aberration arise from specimen preparation due to RI mismatches

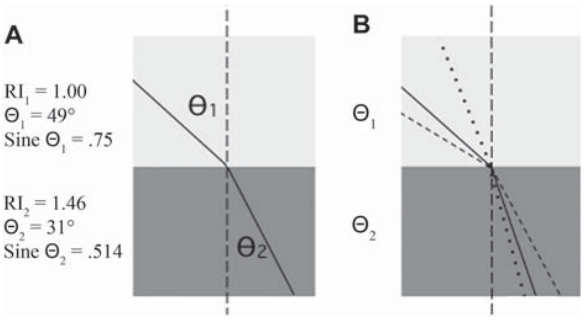

Figure 4. Refraction is illustrated by a light ray passing through two media of different RI, drawn to scale (A). The angles are relative to the optical axis (vertical dashed line); their sines, RI_1 and RI_2, are listed at the left, as determined by Snell's Law. Light rays passing through the interface will refract relative to their angle of incidence (B).

and improper coverslip thickness (see 1–3 for discussion and complete references). The RI of a material is defined as the amount by which the velocity of light passing through the material is reduced relative to vacuum (RI = 1), Table I. A light ray passing through the interface formed by the junction of two media with differing RI will change direction as it changes velocity, a process known as refraction (Figure 4A). The degree of refraction depends on the RI of the media and the sine of the incident angle of the light rays on each side of the interface in a relationship described by Snell's Law (Eq. 1), and illustrated in Figure 4B. This relationship holds regardless of whether a light ray is passing from a higher RI into a lower RI or in the reverse direction.

$$\frac{\sin\Theta_1}{\sin\Theta_2} = \frac{RI_2}{RI_1} \qquad (1)$$

When a lens is focused through an RI interface perpendicular to the optical axis, the light rays are refracted proportionally to their incident angle. The paraxial rays from the center of the objective will be minimally refracted while the high angle marginal rays originating from the edge of the lens will be refracted to the greatest degree. The resulting image will be a blurred superimposition of the images created by rays leaving the objective at different angles and forming foci at different focal planes above or below the expected (nominal) plane of focus. Figure 5A demonstrates an objective lens focused into a medium with the RI for which it was designed; the light rays exiting the margin of the lens at a high angle are focused to the same focal plane as the rays exiting near to the optical axis. However, Figure 5B illustrates the impact of a reduced RI in the specimen shifting the focal plane of the marginal rays towards the coverslip, while the paraxial rays would remain relatively unaffected. The opposite effect would occur in the case where RI_1 was higher than RI_2; the marginal rays would be focused more deeply than the paraxial rays (Figure 36.5 in (12)).

An RI interface is also reflective in a manner proportional to both the magnitude of the square of RI difference at the interface and the angle of incidence, further diminishing signal generation and contrast. Again, this predominately affects rays approaching the interface at high angles collecting the high frequency information essential for resolution. Reflections also reduce contrast by adding scattered light throughout the image. The problem of spherical aberration becomes more troublesome in the presence of multiple interfaces delineating the refractive index variations associated with complex structures such as those found in the mammalian

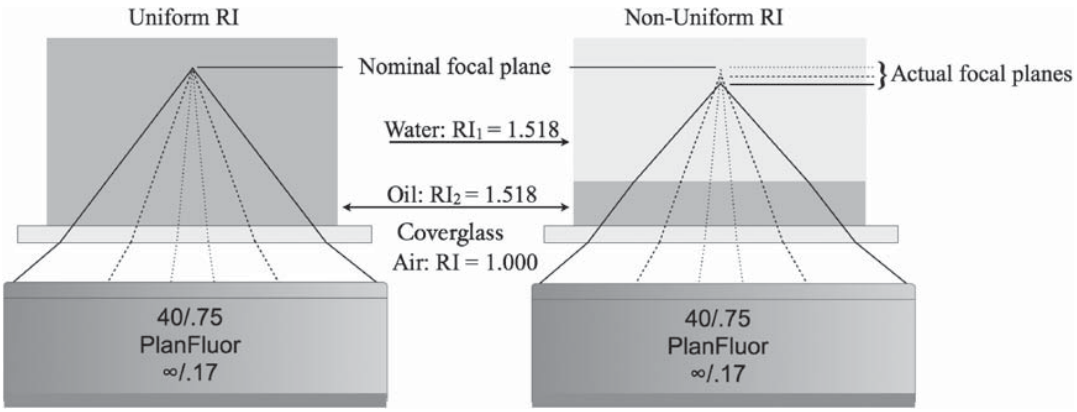

Figure 5. An objective lens is designed to bring light rays from all angles to a nominal plane of focus when focused into a medium possessing the correct RI (A). However, the presence of a layer possessing a different RI will refract the light to focus at different planes depending on the angle at which the ray leaves the objective (B). The RI of the coverglass (1.523) is sufficiently close to that of the RI_1 (1.518), so that refraction becomes negligible.

Table I. Refractive indices for some common media.

Medium	RI
Vacuum	1.0000
Air	1.0003
Water	1.3333
90% glycerol	1.4605
100% glycerol	1.4746
Immersion oil*	1.518
MSBB**	1.556

*Cargille, Type B immersion oil.
**The reported RI varies from 1.536 to 1.5409.

inner ear. The case of an RI interface oriented at some angle relative to the optical axis will also result in a lateral shift of the focus, leading to additional degradation of the image.

MSBB created a sufficiently uniform refractive index throughout the inner ear tissue to render it nearly transparent. The use of an immersion medium closely matched to the high RI of the MSBB further minimized RI variability in the specimen with oil-immersion objectives. Most mounting media commonly used for fluorescence microscopy possess an RI in the range of 1.36–1.49. However, the dense connective tissues of the inner ear's bony structures remain clearly visible by transmitted and reflection light microscopy when mounted in such media, indicating that an RI mismatch exists.

Some correction for RI mismatch is possible by use of special objective lenses equipped with collars that can be adjusted to correct for variations in coverslip thickness. These are predominately very high NA dry objectives or water immersion objectives designed to work with aqueous specimens. A few objectives designated as 'multi-immersion' are equipped with collars to compensate for use with different immersion media to match the RI of specimens over a range of RI from water to immersion oil. Both types of correcting lenses can compensate for a range of RI mismatch between the specimen and the first surface of the objective lens, in addition to coverslip thickness (11). The effect of coverslip thickness is usually not significant with oil-immersion objectives due to the close match in RI between the glass (approx. 1.523) and the immersion oil. A large RI mismatch, such as glass:air or glass:water, can produce significant spherical aberration, where an error in coverslip thickness of 10 μm can result in significant losses of resolution and signal after only 10 μm of focus into the specimen using a high NA dry objective (1). However, lenses having correction collars that allow spherical aberration compensation are not widely available and are extremely costly.

Our labeling method is robust and reproducible, provided the cochlea is subjected to sufficient hydraulic forces to achieve circulation of the antibody throughout the cochlear duct. Incubation with agitation that is too weak, or in containers that do not allow sufficient fluid motion, will fail to label the tissue. Conversely, excessive dissection risks damaging exposed sensory structures if the specimen tumbles freely within the incubation vessel. In general, a degree of dissection that allows access to the lower or mid turns, the apex, the oval and round windows will be sufficient if the combination of vial dimensions, volume and degree of agitation can produce a noticeable wave motion on the surface of the incubation medium.

Type I and type II afferent fibers are known to label for 200 kD neurofilament (13), as are efferent fibers innervating the mouse OHC (14). The small nerve fibers predominately labeled for parvalbumin in this study might be type II afferent fibers based on their relatively small size, arrangement below the OHC, and shape of their synapses (15,16), but they appeared to be unlabeled for 200 kD neurofilament. Nerve fibers of similar appearance and parvalbumin labeling have been reported to be lightly labeled for 200 kD neurofilament (17) using a shorter post-fixation exposure. Differences in antibody specificities and labeling methodologies may be responsible for the range of immunolabeling findings in the inner ear (18). Additional work with combinations of antibodies specific for markers associated with neuronal markers, such as pre- and post-synaptic proteins, would be required to positively identify where these nerve fibers form synapses on the OHC (14,19,20).

The nerve fibers within the modiolar bone and osseous spiral lamina display a dramatic difference in label intensity compared to those that have emerged from the habenula perforata. This suggests inhibition of antibody penetration that may be due to the dense connective tissue or the presence of membranes from myelin sheaths within the modiolar structures.

In summary, a simple means has been presented for reducing the effect of spherical aberrations in fixed preparations of the mammalian inner ear. High quality images may be obtained by confocal microscopy through the full working distance of any objective lens. This method does not require any specialized optics, hardware or custom software. The method is also compatible with deconvolution of three-dimensional optical volumes collected by epifluorescent wide-field microscopy (not shown). Furthermore, this study emphasizes the importance of matching the specimen, the mounting media RI and the coverslip thickness to the requirements of the specific objective lens being utilized in order to

minimize spherical aberration with any mode of light microscopy.

Acknowledgements

Mae del Puerto and Ling Tong provided assistance with specimen fixation, dissections and labeling. Mice were provided by Bronya Keats, Louisiana State University. Elizabeth Oesterle, University of Washington and James Pawley, University of Wisconsin (ret.) provided invaluable insights in review and discussion of this manuscript.

This work was supported by NIDCD grants DC04661, DC03829 and the Foundation Fighting Blindness BR-GE-0606-0347.

Declaration of interest: The authors report no conflicts of interest. The authors alone are responsible for the content and writing of the paper.

References

1. Keller HE. Objective lenses for confocal microscopy. In: Pawley JB, editor. Handbook of Biological Confocal Microscopy, 3rd edn. New York: Springer; 2006.
2. Egner A, Hell SW. Aberrations in confocal and multi-photon fluorescent microscopy induced by refractive index mismatch. In: Pawley JB, editor. Handbook of Biological Confocal Microscopy, 3rd edn. New York: Springer; 2006.
3. Hell S, Reiner G, Cremer C, Stelzer EHK. Aberrations in confocal fluorescence microscopy induced by mismatches in refractive index. J Microsc. 1993;169:391–405.
4. Hardie NA, MacDonald G, Rubel EW. A new method for imaging and 3D reconstruction of mammalian cochlea by fluorescent confocal microscopy. Brain Res. 2004;1000: 200–10.
5. MacDonald GH, Rubel EW. Three-dimensional imaging of the intact mouse cochlea by fluorescent laser scanning confocal microscopy. Hear Res. 2008;243:1–10.
6. Spalteholz W. Über das Durchsichtigmachen von menschlichen und tierischen Präpareten und seine theoretischen Bedingungen. Leipizig: Hirzel; 1914.
7. Voie AH, Burns DH, Spelman FA. Orthogonal-plane fluorescence optical sectioning: three-dimensional imaging of macroscopic biological specimens. J Microsc. 1993;170:229–36.
8. Voie AH. Imaging the intact guinea pig tympanic bulla by orthogonal-plane fluorescence optical sectioning microscopy. Hear Res. 2002;171:119–28.
9. Buytaert JAN, Dirckx JJJ. Design and quantitative resolution measurements of an optical virtual sectioning threedimensional imaging technique for biomedical specimens featuring two-micrometer slicing resolution. J Biomed Optics. 2007;12:014039.
10. Buytaert JAN, Dirckx J. Tomographic imaging of macroscopic biomedical objects in high resolution and three dimensions using orthogonal-plane fluorescence optical sectioning. Appl Optics. 2009;48:941–8.
11. Santi PA, Johnson SB, Hillenbrand M, GrandPre PZ, Glass TJ, Leger JR. Thin-sheet laser imaging microscopy for optical sectioning of thick tissues. BioTechniques. 2009;46:287–94.
12. Hibbs AR, MacDonald G, Garsha K. Practical confocal microscopy. In: Pawley JB, editor. Handbook of Biological Confocal Microscopy. 3rd edn. New York: Springer; 2006.
13. Berlund AM, Ryugo DK. Neurofilament antibodies and spiral ganglion neurons of the mammalian cochlea. J Comp Neurol. 1991;306:393–408.
14. Maison SF, Rosahl TW, Homanics GE, Liberman MC. Functional role of GABAergic innervation of the cochlea: phenotypic analysis of mice lacking $GABA_A$ receptor subunits $\alpha1$, $\alpha2$, $\alpha5$, $\alpha6$, $\beta2$, $\beta3$ or δ. J Neurosci. 2006;26:10315–26.
15. Sato M, Henson MM, Henson OW, Smith DW. The innervation of outer hair cells: 3D reconstruction from TEM serial sections in the Japanese macaque. Hear Res. 1999;135:29–38.
16. Berlund AM, Ryugo DK. Hair cell innervation by spiral ganglion neurons in the mouse. J Comp Neurol. 1987;255: 560–70.
17. Oesterle EC, Campbell S. Supporting cell characteristics in long-deafened aged mouse ears. J Assoc Res Otolaryngol. 2009;10:525–44.
18. Slepecky N, Ulfendahl M. Actin-binding and microtubule associated proteins in the organ of Corti. Hear Res.1992; 57:201–15.
19. Maison SF, Adams JC, Liberman MC. Olivocochlear innervation in the mouse: immunocytochemical maps, crossed versus uncrossed contributions and transmitter colocalization. J Comp Neurol. 2003;455:406–16.
20. Huang L-C, Thome PR, Housley GD, Montgomery JM. Spatiotemporal definition of neurite outgrowth, refinement and retraction in the developing mouse cochlea. Development. 2007;134:2925–33.

Reference to Erratum: Audiological Medicine Mar 2011, Vol. 9, No. 1: 51–51.

Erratum

Three-dimensional Confocal Microscopy of the Mammalian Inner Ear
Glen H MacDonald, Edwin W Rubel

Audiological Medicine 2010, 8(3): 120–128. doi: 10.3109/1651386X.2010.502301

It has come to our attention that this article was published without inclusion of final revisions. The following corrections were omitted:

On page 122 the sentence

> The RI of this clearing mixture was calculated to be 1.556 by multiplying the proportion of each reagent in the final mixture by its RI and summing the results.

Should have read

> The RI of this clearing mixture was calculated to be 1.548 by multiplying the proportion of each reagent in the final mixture by its RI and summing the results.

On page 126 figure 5

> In the figure; "Water: RI1 = 1.518" should have read "Water: RI1 = 1.333".
> The last line of the caption should read "The RI of the coverglass (1.523) is sufficiently close to that of the RI2 (1.518),...".

On page 128 reference 10

> Buytaert JAN, Dirckx J. Tomographic imaging of macroscopic biomedical objects in high resolution and three dimensions using orthogonal-plane fluorescence optical sectioning. Appl Optics. 2009;48:941–8.

Should have read

> Buytaert JAN, Dirckx JJJ. Tomographic imaging of macroscopic biomedical objects in high resolution and three dimensions using orthogonal-plane fluorescence optical sectioning. Appl Optics. 2009;48:941–8.

An incorrect version of Table I was published. The correct version is shown below.

Table 1. Refractive indices for selected mounting/clearing media.

Medium	RI
Water*	1.3333
90% Glycerol (calculated)	1.4605
100% Glycerol*	1.4746
Xylene*	1.494
Immersion oil **	1.518
Methyl salicylate***	1.536
MSBB (calculated)	1.548
Benzyl benzoate*	1.568

* Merck Index, 10th Ed. Rahway(NJ): Merck & Co., Inc; 1983.
** Type B, Cargille Laboratories, Cedar Grove, NJ.
*** Polysciences, Inc, Warrington, PA, Lot #546391. Varies from 1.536 to 1.541.

The editors and authors regret any confusion that may have resulted.